AIAA JOURNAL
Vol. 32, No. 6, June 1994

Effect of Initial Conditions on Vortices in a Turbulent Near Wake

Y. Zhou* and R. A. Antonia†
University of Newcastle, Newcastle, New South Wales 2308, Australia

A study has been made of turbulent vortices behind various wake generating bodies with the same characteristic dimension h (circular, triangular, and square cylinders and a screen of 50% solidity). Using orthogonal arrays of sixteen X wires, eight in the (x, y) plane and eight in the (x, z) plane, velocity data have been obtained simultaneously in the two planes at $x/h = 20$ and $Re\ (\equiv U_0 h/\nu) = 5600$. The topology and transport characteristics of the vortices are sensitive to the initial conditions, in particular on whether the wake-generating body is porous or impervious. For the porous body wake, the vortex strength is only about 30–40% of that in the solid body wakes. The convection velocity and two-dimensional characteristics of the vortices in these two types of flows are also different.

Nomenclature

$\langle B \rangle$ = conditional average of B
C_D = drag coefficient
Co_{uv} = cospectrum of fluctuations u and v
f = frequency
f_0 = most probable vortex frequency
h = characteristic dimension of wake generator (Fig. 1)
N = total number of detections
N_j = number of detections for the jth subset
Q_{uv} = quadrature spectrum of fluctuations u and v
Re = Reynolds number, $\equiv U_0 h/\nu$
t = time
$\overline{U}$ = mean velocity in the streamwise direction
U_c = vortex convection velocity
U_0 = freestream velocity
U_1 = maximum velocity deficit
y_v = most probable lateral position of vortices
β' = root-mean-square value of β
$\tilde{\beta}$ = coherent fluctuation of β
β_r = incoherent fluctuation of β
$\overline{\beta\gamma}$ = structural average of $\beta\gamma$
Γ_0 = vortex strength
δ = mean velocity half-width
ν = kinematic viscosity
ρ = correlation coefficient
ϕ_{uv} = phase in the cross spectrum of u and v
Ω_z = azimuthally averaged spanwise vorticity, defined in Eq. (3)
Ω_{z0} = maximum value of Ω_z
ω_z = instantaneous spanwise vorticity
ω_{zp} = local peak value of ω_z

I. Introduction

THE effect of the initial conditions on the behavior of a plane wake has been investigated by a number of authors. Sreenivasan[1] observed substantial differences in the manner wakes produced by different generators evolved, even though the shape of the mean velocity profile remained the same (when normalized by its own characteristic scales) in each case. Sreenivasan and Narasimha[2] suggested that a unique self-preserving state existed for all plane wakes. Wygnanski et al.[3] reported a dependence of the normalized distributions of the longitudinal turbulence intensity on the initial conditions over a distance 100–2000 momentum thicknesses downstream of the wake generator. The more recent studies of Louchez et al.,[4] Cimbala et al.,[5] and Matsumura et al.[6] have confirmed that the detailed behavior of a turbulent wake (both near and far fields) is strongly dependent on the initial conditions. This, in effect, suggests that the characteristics of the vortical motion in the wake may differ as the initial conditions differ. This difference does not seem to have been well documented, although Matsumura et al. compared the spectral behaviors, topology, and transport characteristics (i.e., coherent and incoherent contributions to the Reynolds stresses) of the near wake of a screen (60% solidity) with that behind a solid plate. They concluded that they were "definitely not the same."

In the present study, vortices behind various wake-generating bodies have been examined in some detail with the objective of assessing their sensitivity to initial conditions. The experimental methodology that is adopted consists in first detecting the vortices by a procedure that includes criteria for the vorticity concentration and circulation. The velocity field is subsequently conditioned with respect to the detection instants, thus allowing the comparison of conditional sectional streamlines and vorticity contours obtained with each wake generator. The contributions the vortices make to the Reynolds stresses have been quantified in each case. The effect of initial conditions on the strength, convection velocity, and two-dimensionality of the vortices is also considered.

II. Experimental Details

Experiments were carried out in an open-return low-turbulence wind tunnel with a 2.4-m-long working section (0.35 × 0.35 m). The bottom wall was tilted to achieve a zero streamwise pressure gradient. Various wake generators (circular, triangular, and square cylinders and a screen of 50% solidity) of the same height (h = 12.5 mm) were used. Each generator was installed in the midplane and spanned the full width of the working section, 20 cm from the exit plane of the contraction. This resulted in a blockage of about 3.6%. Measurements were made at $x/h = 20$ and a Reynolds number of 5.6×10^3.

Orthogonal arrays of sixteen X-wire probes (see Fig. 1 for spatial arrangement) were used for the simultaneous measurement of velocity fluctuations u and v in the (x, y) plane and u and w in the (x, z) plane ($y/h \simeq 0.7$). The nominal spacing between X wires in both planes was about 5 mm except for a relatively large gap of 9.1 mm between the fourth and fifth X wires in the (x, z) plane. The arrays were attached to separate traversing mechanisms and could be moved independently of each other. The physical blockage caused by these arrays,

Received Jan. 9, 1993; revision received Nov. 5, 1993; accepted for publication Nov. 8, 1993.

*Research Associate, Department of Mechanical Engineering.
†Professor, Department of Mechanical Engineering.

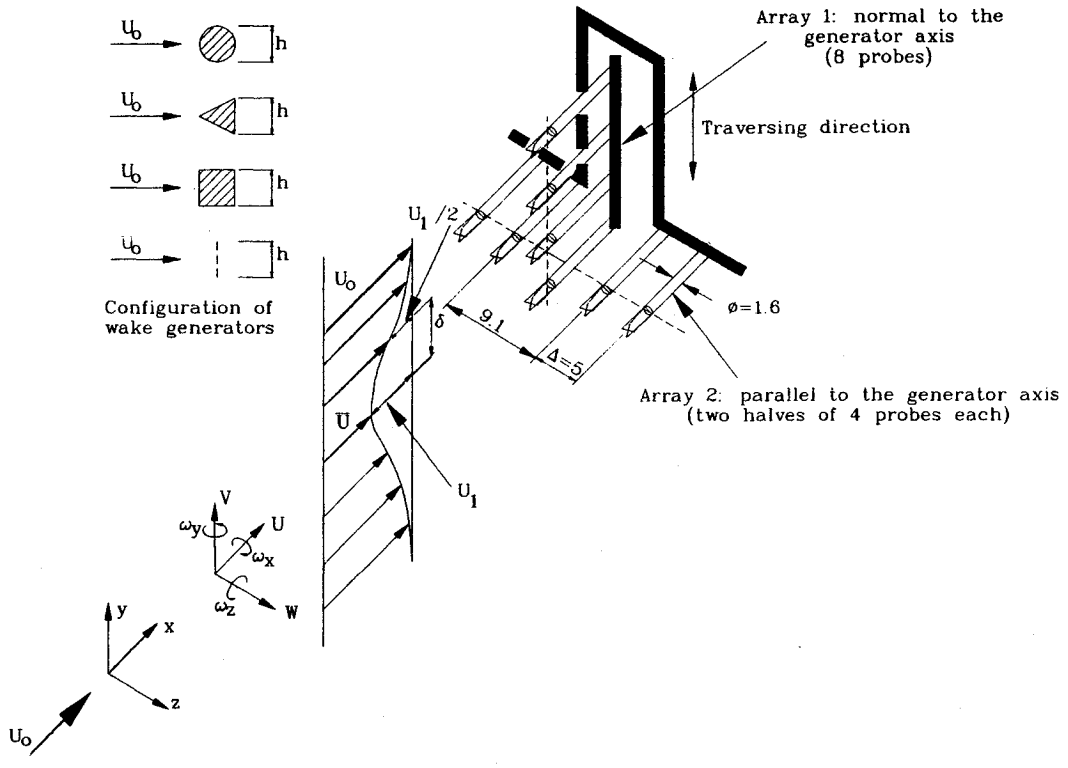

Fig. 1 Experimental arrangement.

cables, and supports was estimated to be about 3%. Several types of measurements (not presented here) indicated that the interference to the flow due to the two arrays was negligible.

Wollaston (Pt-10% Rh) wires, 5 μm in diameter and about 1 mm in working length, were operated with constant temperature circuits. Signals from the circuits were offset, amplified, and then digitized using two 16-channel (12-bit) analogue-to-digital boards and two personal computers (NEC 386) at a sampling frequency of 3.5 kHz per channel. Data acquisition by the two computers was synchronized using a common external trigger pulse (the configuration is shown in Ref. 7). Using velocity and yaw calibrations, signals proportional to u, v, and w, together with the local mean velocities $\overline{U}$ and $\overline{V}$ ($\simeq 0$) and $\overline{W}$ ($\simeq 0$), were formed on digital tape. The duration of each record was about 38 s. Subsequent data processing was done on a VAX 8550 computer.

III. Vortex Detection

Vortices are identified—with respect to both time and lateral locations—by a method that includes criteria for vorticity concentration and circulation. Only a brief description is given here (more details are given in Ref. 8). Using instantaneous signals $U = \overline{U} + u$ and $V = \overline{V} + v = v$, an approximation to the instantaneous spanwise vorticity is

$$\omega_z \simeq \frac{\Delta V}{\Delta x} - \frac{\Delta V}{\Delta y}$$

where $\Delta y \simeq 5$ mm is the spacing between X wires and $\Delta x = -0.87\ U_0 \Delta t$. The value $0.87\ U_0$ is the assumed convection velocity; this value is not critical for determining vortex locations.[8]

In the first criterion, the local peak values of ω_z and ω_{zp}, for instance, are compared with the maximum mean shear $S_m = (\partial \overline{U}/\partial y)_{\max}$. Specifically, a detection is first assumed to occur when

$$|\omega_{zp}| > k_\omega S_m \tag{1}$$

In Eq. (1), k_ω is a positive threshold, which is at first chosen arbitrarily and later modified after visually examining detection locations on instantaneous vorticity contour plots.

Before the second criterion is applied, the circulation Γ is calculated using the following equation:

$$\Gamma = \int_0^{r_v} \left[\int_0^{2\pi} \omega_z(r, \theta)\, d\theta \right] r\, dr \tag{2}$$

where $\omega_z(r, \theta)$ is obtained by applying a surface-fit technique to vorticity data centered on ω_{zp} (i.e., the origin of the r, θ coordinate system is at the location of ω_{zp}). In Eq. (2), r_v is the vortex radius where the mean vorticity at a radius r from the vortex center, defined by

$$\Omega_z(r) = \frac{1}{2\pi} \int_0^{2\pi} \omega_z(r, \theta)\, d\theta \tag{3}$$

drops to the assumed minimum vorticity level $\Omega_{zc}(>0)$ for the vortex, viz.,

$$|\Omega_z(r_v)| = \Omega_{zc} \tag{4}$$

Equation (4) is solved for r_v by using a quasi-Newton optimizing algorithm[9] that searches for the minimum of $[|\Omega_z(r)| - \Omega_{zc}]^2$. The magnitude of Γ determined from Eq. (2) is required to satisfy the following condition:

$$|\Gamma| \geq k_\Gamma S_m h^2 \tag{5}$$

where k_Γ is a positive threshold determined in similar fashion to k_ω.

By varying k_ω and k_Γ, the number of detections is chosen to be about 2000 for the circular and triangular cylinders, 1400 for the square cylinder, and 2800 for the screen. These numbers correspond to a detection frequency of half the vortex frequency f_0, which is identified by the location of the main peak in the v spectrum (Fig. 2). Note that for the porous body wake a bump centered at a Strouhal number of $f_0 h/U_0 \simeq 0.28$ is clearly distinguishable, indicating the existence of quasi-

periodic vortices. The spread of the bump contrasts with the relatively sharp peak observed for the solid body wakes.

IV. Conditional and Structural Averages

The conditional average of an instantaneous quantity B is given by

$$\langle B\rangle_k = \frac{1}{N}\sum_{m=1}^{N} B_{j_m+k}$$

where k represents time (in samples, positive or negative) relative to the detection points j_m. (For convenience, the subscript k will be omitted.) The conditional average of $\Omega_z(r)$ defined by Eq. (3) is specifically defined by

$$\langle\Omega_z\rangle(r) = \frac{1}{N}\sum_{m=1}^{N}\Omega_{zm}(r)$$

The variable B can be viewed as the sum of the time mean component $\overline{B}$ and the fluctuation component β. The latter can be further decomposed into the coherent fluctuation $\tilde{\beta} \equiv \langle\beta\rangle$ and a remainder β_r, viz.,

$$\beta = \tilde{\beta} + \beta_r$$

Also

$$\langle\beta\gamma\rangle = \tilde{\beta}\tilde{\gamma} + \langle\beta_r\gamma_r\rangle \tag{6}$$

where β and γ can each stand for either u or v.

If the conditionally averaged structure begins k_1 samples before the detection instant and ends k_2 samples after this instant, a structural average is denoted by a double overbar, e.g.,

$$\overline{\overline{\tilde{\beta}\tilde{\gamma}}} = \frac{1}{k_1+k_2+1}\sum_{-k_1}^{k_2}\tilde{\beta}\tilde{\gamma} \tag{7}$$

The value of $k_1(=k_2)$ is 15 for the circular and triangular cylinder wakes, 25 for the square cylinder wake, and 11 for the porous body wake, so that the duration (k_1+k_2+1) corresponds to approximately the average time interval between structures in each flow.

V. Results

Figure 3 shows that the lateral distributions of $\overline{U}$, $\overline{u^2}$, $\overline{v^2}$, and $\overline{uv}$ depend on the initial conditions. The maximum velocity deficit U_1 is larger for the porous body than for the solid bodies for which U_1 varies by a relatively small amount. The solid body wakes, in particular that of the square cylinder, have considerably larger values of $\overline{u^2}$ and $\overline{v^2}$ than the porous body wake. The maximum value of $\overline{uv}$ in the porous body wake is comparable to that for the circular cylinder but smaller than for the other two wakes.

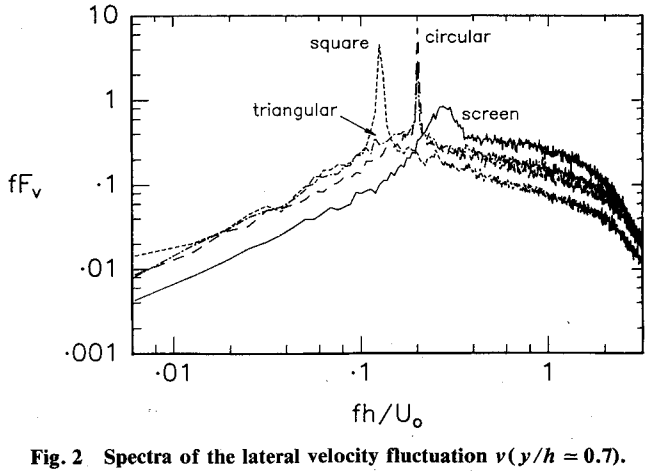

Fig. 2 Spectra of the lateral velocity fluctuation $v(y/h = 0.7)$.

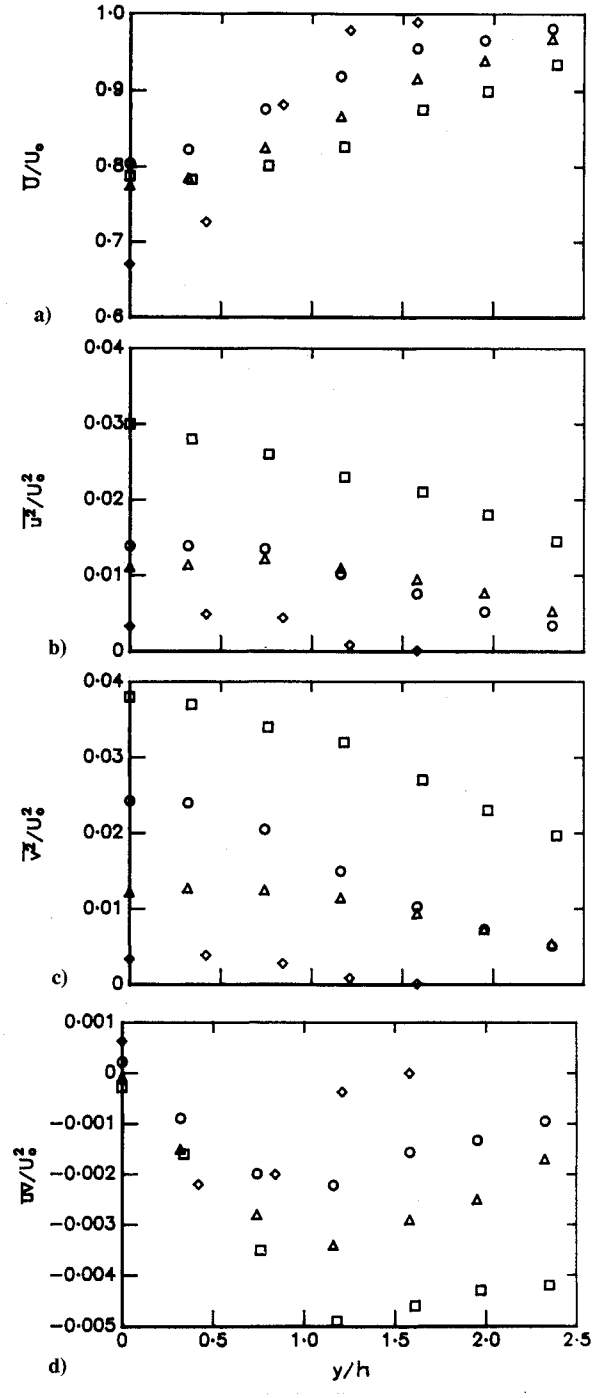

Fig. 3 Lateral distributions of mean velocity and Reynolds stresses: a) $\overline{U}/U_0$, b) $\overline{u^2}/U_0^2$, c) $\overline{v^2}/U_0^2$, and d) $\overline{uv}/U_0^2$; $(x/d = 20)$; ○, circular cylinder; △, triangular; □, square; ◇, screen.

Table 1 lists some characteristic properties of wakes. The drag coefficient C_D may be calculated from the relation[10]

$$C_D = 4\int_0^\infty\left(\frac{U_0-\overline{U}}{U_0}\right)\frac{\overline{U}}{U_0}\,d\left(\frac{y}{h}\right) + 4\int_0^\infty\frac{\overline{v^2}-\overline{u^2}}{U_0^2}\,d\left(\frac{y}{h}\right) \tag{8}$$

Although U_1 is largest for the porous body wake, C_D is, as expected, smallest for this flow. The decrease in C_D is primarily caused by the first term in Eq. (8), due to a relatively small mean velocity half-width δ, rather than by the second term that is negligibly small in magnitude and negative in sign. The present C_D estimate for the circular cylinder is in good agreement with earlier estimates, e.g., Roshko[11] ($C_D = 1.0$), Browne et al.[12] ($C_D = 0.97$), and Antonia and Rajagopalan[10]

($C_D \simeq 0.86$). For the square cylinder wake, C_D is slightly smaller than Lee's[13] estimate ($\simeq 2.0$).

A few properties of the detected vortices are summarized in Table 2. The vortex frequency f_0 for the porous body wake is largest corresponding to a Strouhal number of about 0.28. This number is about 0.2 for the circular and triangular cylinders and 0.12 for the square cylinder. This latter value is the same as that reported by Vickery.[14]

The convection velocity $\langle U_c \rangle$ is given by the mean velocity at the vortex centers that are located on the most probable lateral position y_v, i.e., along the vortex path. The value of y_v is estimated from a histogram (not shown here) of the lateral distribution of detections. In the porous body wake, $\langle U_c \rangle$ ($\simeq \overline{U}$) is noticeably smaller than in solid body wakes. For a circular cylinder wake, Zhou and Antonia[8,15] found that $\langle U_c \rangle$ is greater than $\overline{U}$ and attributed this difference to the interaction between the opposite-signed vortices. This interaction, however, appears to be very weak in the porous body wake, as indicated by the conditional sectional streamlines presented later in this section.

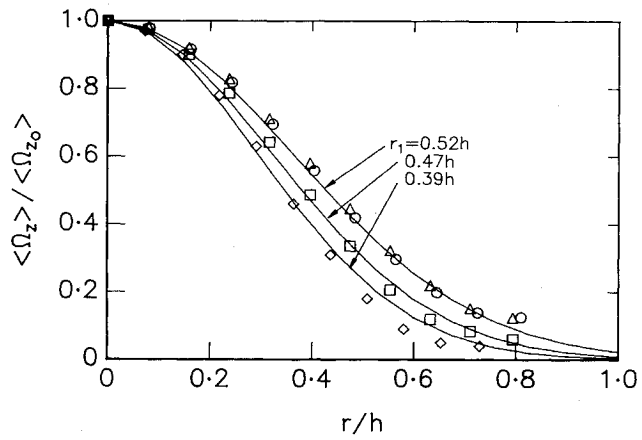

Fig. 4 Conditional vorticity distribution of $\langle \Omega_z \rangle(r)$: ——, $\exp(-1.26r^2/r_1^2)$; ○, circular cylinder; Δ, triangular; □, square; ◇, screen.

The ratio $\langle \Omega_z \rangle(r)/\langle \Omega_{z0} \rangle$ is reasonably well approximated by an exponential distribution $\langle \Omega_z \rangle/\langle \Omega_{z0} \rangle = \exp(-1.26r^2/r_1^2)$, where r_1 is a constant (Fig. 4). Therefore, the vortex strength Γ_0 may be estimated[8] using an Oseen vortex model, i.e., $\Gamma_0 = \pi \langle \Omega_{z0} \rangle r_1^2/1.26$. Obviously, Γ_0 is related to the peak value and distribution of vorticity, which are in general different for different wake generators. As a result, the vortex strengths may also vary. This variation is small among different solid body wakes but considerably large between solid and porous body wakes. The vortex strength in the porous body wake is only about 30–40% of that in the solid body wakes.

Another difference between vortices in porous and solid body wakes is the phase shift between u and v, given by $\phi_{uv}(f_0) \equiv \tan^{-1}[Q_{uv}(f_0)/C_{uv}(f_0)]$. The magnitude of $\phi_{uv}(f_0)$ is close to 90 deg for solid body wakes but close to 180 deg for the porous body wake. This implies that the coherent contribution to the Reynolds shear stress ($\overline{uv}$) may be small in solid body wakes but significant in porous body wakes. Results presented later in this section corroborate this implication.

Conditional sectional streamlines (Fig. 5) and vorticity contours (Fig. 6) based on detections along the vortex path suggest that the geometrical characteristics of the vortex street, e.g., shape, size, and spacing of the vortices, vary from wake to wake, the major variation being observed between porous and solid body wakes. Presumably, the characteristics are dictated, to a large extent, by the dynamics of vortex formation. For solid body wakes, the shedding process that is responsible for the production of vortices should be affected by the overall geometry of the generators. For example, one would expect that the separation points are more clearly de-

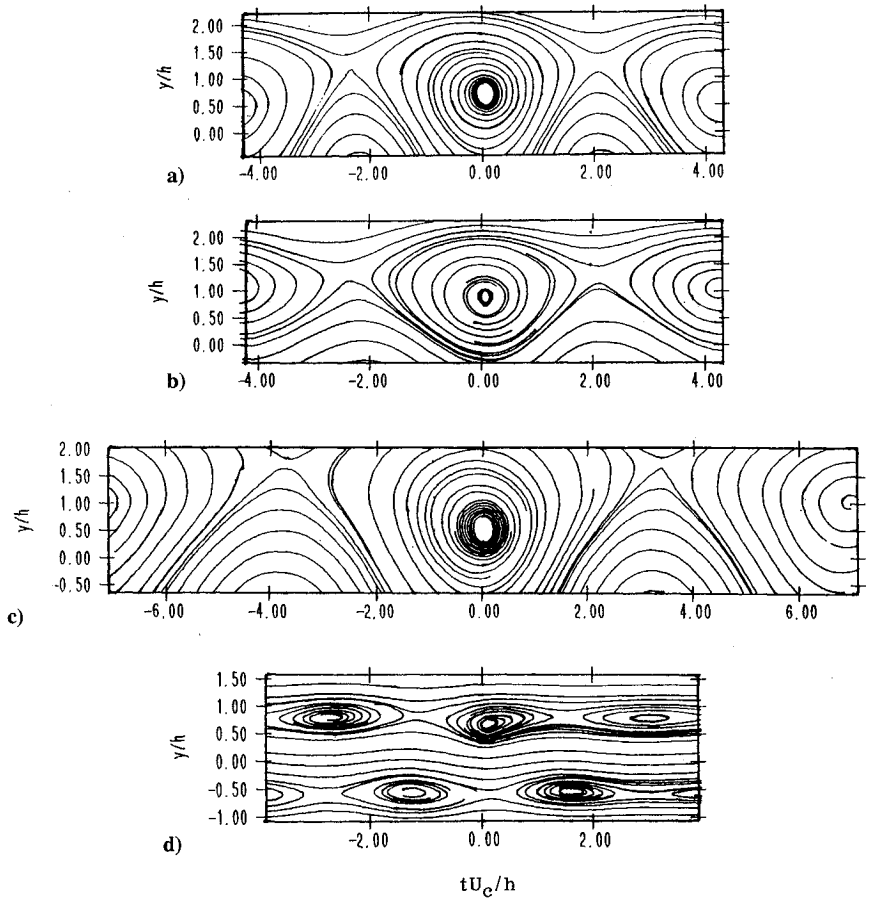

Fig. 5 Conditional sectional streamlines: a) circular cylinder, b) triangular cylinder, c) square cylinder, and d) screen.

Table 1 Characteristic properties of different wakes

Wake generator	C_D	U_1/U_0	δ/h
Circular cylinder	0.95	0.20	1.12
Triangular cylinder	1.20	0.22	1.43
Square cylinder	1.70	0.22	1.54
Screen	0.66	0.33	0.81

fined for the triangular and square cylinders than for the circular cylinder. This implies that the degree of spatial uniformity exhibited by the vortex streets will differ. Castro[16] showed that the vortex street disappears when the solidity of screen is less than about 80%. Zdravkovich[17] investigated the development of the wake behind a set of three circular cylinders. He observed a new vortex street following the decay of the initial vortex street. The formation of this secondary vortex street was explained in terms of a shear layer instability (he also referred to a rolling-up process induced by distributed vorticity). It seems plausible that the mechanism responsible for the vortex formation in the porous body near wake is similar to that which prevails for the secondary vortex street. This would explain the significant difference between the near wake of a porous body and that of a solid body. It would also be compatible with the similarity between the porous body near wake and the far wake (of both solid and porous bodies). Note that vortices in the porous body wake occur in a quasi-periodic fashion and alternate on either side of the centerline, as observed by Matsumura et al.[6] ($Re = 1.1 \times 10^4$, $x/h = 24$). Similar observations have been made for the fully developed plane jet[18] and the far wake of a circular cylinder.[19] Speculatively, the vortex formation mechanism is similar in these flows.

The distributions of $\overline{\tilde{u}^2}$, $\overline{\tilde{v}^2}$, and $\overline{\tilde{u}\tilde{v}}$ in Fig. 7 give some idea of the coherent contribution to the Reynolds stresses (cf. $\overline{u^2}$, $\overline{v^2}$, and $\overline{uv}$ in Fig. 3). It has already been noted that the lateral location of vortices may vary considerably, especially for solid body wakes. Conditional quantities, particularly those associated with u, e.g., $\tilde{u}$ and $\tilde{u}\tilde{v}$, will therefore be smeared or underestimated if vortices are aligned only with respect to time (thus ignoring the jitter in their y locations). To reduce this smearing, vortices have been separated into five subsets according to their lateral location, and $\overline{\tilde{f}\tilde{g}}$ in Fig. 7 is calculated from

$$\overline{\tilde{f}\tilde{g}} = \sum_{j=1}^{5} \frac{N_j}{N} (\overline{\tilde{f}\tilde{g}})_j \qquad (9)$$

where $(\overline{\tilde{f}\tilde{g}})_j$ is the structural average of the jth subset. For all of the structural averages presented here, it has been verified that $\langle \overline{\tilde{f}\tilde{g}} \rangle$ is approximately equal to $\overline{fg}$ (the maximum departure is of order 10%), implying that the detections are reasonably representative of the flow. Figure 7 indicates that the maximum values of the structural averages tend to occur approximately along the vortex path ($y/h \simeq 0.5$–0.7), although the maximum value of $\overline{\tilde{u}^2}$ for the solid body wakes occurs slightly above the vortex path ($y/h \simeq 0.7$–1.2).

The maximum (percentage) values of $\overline{\tilde{f}\tilde{g}}/\overline{fg}$ are shown in Table 3. The coherent contribution to $\overline{v^2}$ is almost twice that of $\overline{u^2}$. This may be related to the considerably larger uncertainty of vortex location in the lateral direction ($= \pm 0.5$ X-wire spacing $\simeq \pm 2.5$ mm) than in the longitudinal direction ($= \pm 0.5 U_c$/sampling frequency $\simeq \pm 0.8$ mm for solid body wakes). This large uncertainty will inevitably result in $\tilde{u}$ and hence $\overline{\tilde{u}^2}$ and $\overline{\tilde{u}\tilde{v}}$ being underestimated despite the use of Eq. (9). Table 3 indicates that the coherent contribution to $\overline{u^2}$ and $\overline{v^2}$ is higher in solid body wakes (30–70%) than in the porous body wake (20–40%). This and the fact that the solid body vortices have a circulation that is considerably larger than the porous body vortices (Table 2) suggest that the former vortices contain more energy than the latter vortices. The contribution to $\overline{uv}$ is, however, smaller for solid body wakes (5–20%) than for the porous body wake ($\simeq$40%). Speculatively, vortices that are shed from solid body wakes

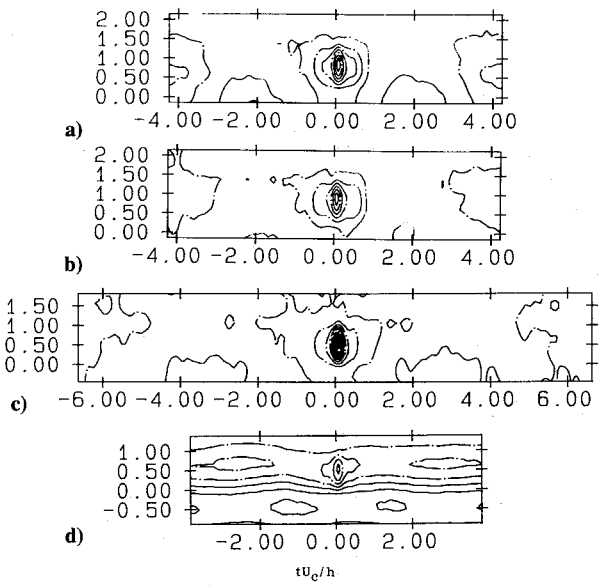

Fig. 6 Conditional vorticity contours, $\langle \omega_z \rangle h/U_0$ (contour increment = 0.2): a) circular cylinder (−1.3 to +0.3), b) triangular (−1.1 to +0.1), c) square (−1.7 to +0.1), and d) screen (−0.8 to +0.4).

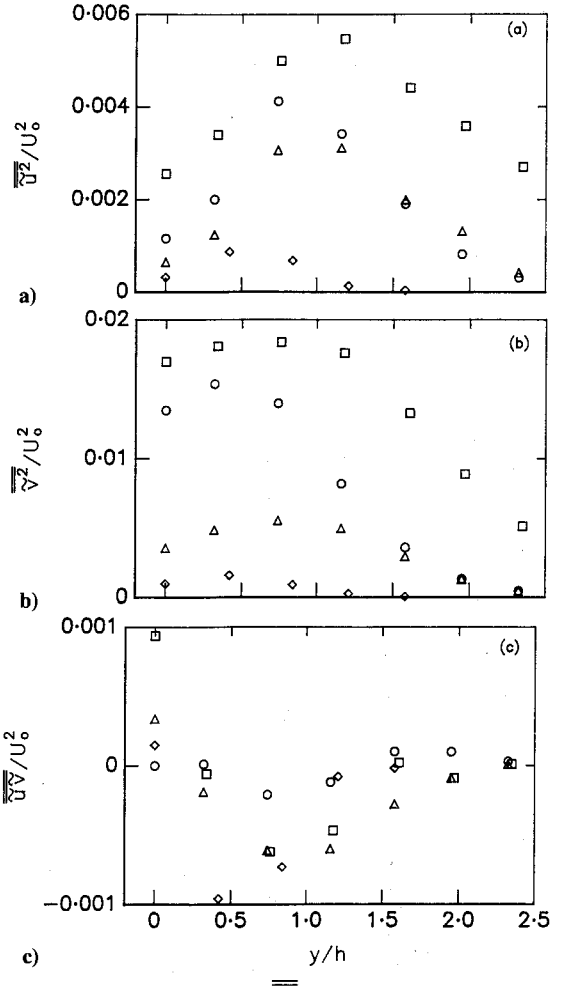

Fig. 7 Coherent contributions $\overline{\tilde{\beta}\tilde{\gamma}}/U_0^2$ to Reynolds stresses: a) $\beta = \gamma = u$, b) $\beta = \gamma = v$, and c) $\beta = u$, $\gamma = v$: ○, circular cylinder; △, triangular; □, square; ◇, screen.

are strongly rotational, as suggested by the relatively large values of $\langle \Gamma_0 \rangle$ in Table 2. In addition, they may also be quite energetic (see $\overline{\tilde{u}^2}/\overline{u^2}$ and $\overline{\tilde{v}^2}/\overline{v^2}$ in Table 3), implying they may not be significantly affected by the incoherent turbulence. Consequently, they are likely to resemble Oseen vortices[8] with

Table 2 Some characteristic properties of vortices

Wake generator	y_v/h	$\langle U_c\rangle/U_0$	$\lvert\langle\omega_{zp}\rangle\rvert h/U_0$	$\lvert\langle\Gamma_0\rangle\rvert/U_0h$	f_0h/U_0	$\phi_{uv}(f_0)$
Circular cylinder	0.5	0.87	1.63	0.88	0.21	−94°
Triangular cylinder	0.9	0.85	1.34	0.72	0.21	−72°
Square cylinder	0.7	0.85	2.05	1.00	0.12	−112°
Screen	0.7	0.78	0.95	0.30	0.28	−169°

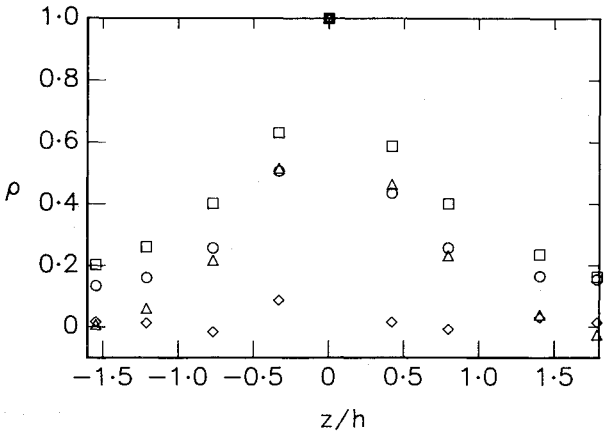

Fig. 8 Variation of ρ with z/h: ○, circular cylinder; Δ, triangular; □, square; ◇, screen.

relatively weak contributions to $\overline{uv}$. On the other hand, vortices in the porous body wake are less rotational and energetic (Tables 2 and 3) and more likely to be influenced by the incoherent turbulence. Their contribution to $\overline{uv}$ should therefore be significant. The difference between solid and porous body wakes—with respect to the different coherent contributions to $\overline{uv}$—is also consistent with the observed phase shift between u and v in these two types of flow. For solid body wakes, $\phi_{uv}(f_0)$ is close to 90 deg (Table 2), and the average value of the uv product tends to be minimized; for the porous body wake, however, $\phi_{uv}(f_0)$ is close to 180 deg, and the magnitude of this product tends to be maximized.

Figure 8 shows the spanwise variation of the correlation coefficient, viz.,

$$\rho = \frac{\overline{u_{z=0}u}}{u'_{z=0}u'} \tag{10}$$

between u signals from the X wires in the (x, z) plane and the u signal, denoted by $u_{z=0}$, from the X wire in the (x, y) plane that is closest to the (x, z) plane. The variation of ρ gives some indication of the two-dimensionality of the flow. Figure 8 shows that the rate of decrease of ρ with $|z|/h$ depends on the wake generator. For example, at $|z|/h \simeq 0.4$, ρ is less than 0.1 for the porous body wake, compared with 0.5–0.6 for the others, implying that the vortices appear much less two-dimensional for the porous than the solid body wakes. This may also be attributed to the different formation mechanisms of the vortices. As speculated previously, vortices in the porous body wake may result from a mechanism involving a shear layer instability. The vortex formation associated with this mechanism is more likely to occur locally in both space and time. The resulting vortices are therefore likely to exhibit less periodicity and smaller length scales, especially in the spanwise direction, than those that result from a shedding mechanism.

Conclusions

The behavior of vortices in wakes from two-dimensional bodies depends on the initial conditions. The difference between porous and solid body wakes is particularly noticeable. For example, the phase shift at the vortex shedding frequency between u and v is close to 180 deg in the porous body wake but close to 90 deg in the solid body wakes. The vortex strength in the former is only 30–40% of that in the latter. Significant differences in the convection velocity and two-dimensionality of the vortices are also observed between the two types of wakes. It is suggested that these differences reflect basic differences in the vortex formation mechanisms. Vortices in solid body wakes are shed from the body surface, whereas those in the porous body wake are likely to arise from an instability in the developing mean wake profile (Cimbala et al.[5]). The topology and transport properties of the vortices in the two types of wakes are accordingly quite different. Vortices in solid body wakes contribute more to the Reynolds normal stresses but considerably less to the Reynolds shear stress than those in the porous body wake.

Table 3 Maximum coherent contributions (%) to Reynolds stresses

Wake generator	$\overline{\tilde{u}^2}/\overline{u^2}$	$\overline{\tilde{v}^2}/\overline{v^2}$	$\overline{\tilde{u}\tilde{v}}/\overline{uv}$
Circular cylinder	34	68	4
Triangular cylinder	28	44	21
Square cylinder	28	55	18
Screen	18	41	44

Acknowledgments

The support of the Australian Research Council is gratefully acknowledged. The authors also acknowledge J. Mi's contribution to all of the experimental work.

References

[1]Sreenivasan, K. R., "Approach to Self-Preservation in Plane Turbulent Wakes," *AIAA Journal,* Vol. 19, No. 10, 1981, pp. 1365–1367.

[2]Sreenivasan, K. R., and Narasimha, R., "Equilibrium Parameters for Two Dimensional Turbulent Wakes," *Journal of Fluids Engineering,* Vol. 104, 1982, pp. 167–170.

[3]Wygnanski, I., Champagne, F., and Marasli, B., "On the Large-Scale Structures in Two-Dimensional, Small-Deficit, Turbulent Wakes," *Journal of Fluid Mechanics,* Vol. 168, July 1986, pp. 31–71.

[4]Louchez, P. R., Kawall, J. G., and Keffer, J. F., "Detailed Spread on Characteristics of Plane Turbulent Wakes," *Proceedings of the 5th Symposium on Turbulent Shear Flows,* Lecture Notes in Physics, Springer-Verlag, Berlin, 1987, pp. 98–109.

[5]Cimbala, J. M., Nagib, H. M., and Roshko, A., "Large Structure in the Far Wakes of Two-Dimensional Bluff Bodies," *Journal of Fluid Mechanics,* Vol. 190, May 1988, pp. 265–298.

[6]Matsumura, M., Huang, Z., Kawall, J. G., and Keffer, J. F., "Coherent Structures in the Turbulent Wake of a Porous Body," *Proceedings of the Eighth Symposium on Turbulent Shear Flows,* Technical Univ. of Munich, Munich, Germany, 1991, pp. 28-2-1–28-2-6.

[7]Krogstad, P.-Å., Antonia, R. A., and Browne, L. W. B., "Structure Investigation in a Turbulent Boundary Layer Using Orthogonal X-Wire Arrays," *Proceedings of the Australasian Fluid Mechanics Conference,* Univ. of Tasmania, Hobart, Australia, 1992, pp. 251–254.

[8]Zhou, Y., and Antonia, R. A., "A Study of Turbulent Vortices in the Near-Wake of a Cylinder," *Journal of Fluid Mechanics,* Vol. 253, Aug. 1993, pp. 643–661.

[9]Gill, P. E., and Murray, W., "Minimization Subject to Bounds on the Variations," National Physical Lab., Rept. NAC 72, London, 1976.

[10]Antonia, R. A., and Rajagopalan, S., "A Comment on the Determination of Drag of a Circular Cylinder," *AIAA Journal,* Vol. 28, No. 10, 1990, pp. 1833, 1834.

[11]Roshko, A., "On the Wake and Drag of Bluff Bodies," *Journal of the Aeronautical Sciences,* Vol. 22, Feb. 1955, pp. 124–132.

[12]Browne, L. W. B., Antonia, R. A., and Shah, D. A., "Turbulent Energy Dissipation in a Wake," *Journal of Fluid Mechanics,* Vol.

179, June 1987, pp. 307–326.

[13]Lee, B. E., "The Effect of Turbulence on the Surface Pressure Field of a Square Prism," *Journal of Fluid Mechanics,* Vol. 69, Pt. 2, 1975, pp. 263–282.

[14]Vickery, B. J., "Fluctuating Lift and Drag on a Long Cylinder of Square Cross-Section in a Smooth and Turbulent Stream," *Journal of Fluid Mechanics,* Vol. 25, Pt. 3, 1966, pp. 481–494.

[15]Zhou, Y., and Antonia, R. A., "Convection Velocity Measurements in a Cylinder Wake," *Experiments in Fluids,* Vol. 13, No. 1, 1992, pp. 63–70.

[16]Castro, I., "Wake Characteristics of Two-Dimensional Perforated Plates Normal to an Air-Stream," *Journal of Fluid Mechanics,* Vol. 46, Pt. 3, 1971, pp. 599–609.

[17]Zdravkovich, M. M., "Smoke Observations of the Wake of a Group of Three Cylinders at Low Reynolds Number," *Journal of Fluid Mechanics,* Vol. 32, Pt. 2, 1968, pp. 339–351.

[18]Chambers, A. J., Antonia, R. A., and Browne, L. W. B., "Effect of Symmetry and Asymmetry of Turbulent Structures on the Interaction Region of a Plane Jet," *Experiments in Fluids,* Vol. 3, No. 6, 1985, pp. 343–348.

[19]Bisset, D. K., Antonia, R. A., and Browne, L. W. B., "Spatial Organization of Large Structures in the Turbulent Far Wake of a Cylinder," *Journal of Fluid Mechanics,* Vol. 218, Sept. 1990, pp. 439–461.